LY294002 alleviates bone cancer pain by reducing mitochondrial dysfunction and the inflammatory response

JIAJIA ZHAO[1*], YING YAN[2*], SHUQING ZHEN[3*], LIANGZHU YU[1], JIEQIONG DING[1], QIONG TANG[1], LING LIU[1], HAILI ZHU[1] and MIN XIE[1]

[1]Xianning Medical College, Hubei University of Science and Technology, Xianning, Hubei 437100; [2]Xishui Hospital Affiliated to Hubei University of Science and Technology, Huanggang, Hubei 438299; [3]Matang Hospital of Traditional Chinese Medicine, Xianning, Hubei 437020, P.R. China

Received November 8, 2022; Accepted March 17, 2023

DOI: 10.3892/ijmm.2023.5245

Abstract. Bone cancer pain (BCP) is mainly caused by bone metastasis and markedly impairs the functional capacity and daily functions of patients. Neuroinflammation plays a pivotal role in the pathogenesis and maintenance of chronic pain. Oxidative stress in the mitochondria is a key contributor to neuroinflammation and neuropathic pain. Herein, a rat model of BCP was established which was characterized by bone destruction, pain hypersensitivity and motor disability. In the spinal cord, phosphatidylinositol 3-kinase (PI3K)/protein kinase B (Akt) signaling was activated, and the inflammatory response and mitochondrial dysfunction were also observed. The intrathecal injection of LY294002, a selective inhibitor of PI3K/Akt signaling, decreased mechanical pain sensitivity, suppressed spontaneous pain and recovered the motor coordination of rats with BCP. Second, LY294002 treatment blocked spinal inflammation by reducing astrocytic activation and downregulating the expression levels of inflammatory factors, such as NF-κB, IL-1β and TNF-α. Moreover, LY294002 treatment recovered mitochondrial function by activating the manganese superoxide dismutase enzyme, increasing NADH:ubiquinone oxidoreductase subunit B11 expression, and decreasing BAX and dihydroorotate dehydrogenase expression. LY294002 treatment also increased the mitochondrial membrane potential and decreased the mitochondrial reactive oxygen species levels in C6 cells. On the whole, the results of the present study suggest that the inhibition of PI3K/Akt signaling by LY294002 restores mitochondrial function, suppresses spinal inflammation and alleviates BCP.

Correspondence to: Dr Haili Zhu or Dr Min Xie, Xianning Medical College, Hubei University of Science and Technology, 88 Xianning Road, Xianning, Hubei 437100, P.R. China
E-mail: hkhaili_zhu@163.com
E-mail: xiemin2020a@163.com

*Contributed equally

Key words: bone cancer pain, spinal inflammation, mitochondrial oxidative stress, LY294002, phosphatidylinositol 3-kinase/protein kinase B signaling

Introduction

Bone cancer pain (BCP) is a significant and life-altering pain, and is the most common symptom of bone metastasis, which occur in almost all types of cancer. Among all the cancer types, the relative incidence of breast, prostate and thyroid cancer is 75, 75 and 40%, respectively (1). It was estimated that there were 19.3 million new cancer cases in 2020, according to the GLOBOCAN 2020 database (2). Moreover, the 5-year relative survival rate of cancer patients increases to 68%, depending on the advanced treatment and improved diagnoses. However, 60-84% of patients with advanced-stage cancer experience varying degrees of bone pain (3). The mainly clinical symptoms of BCP are stable background pain, occasional breakthrough pain and ongoing pain (4). BCP is described by patients as annoying, gnawing, aching and nagging, and is exacerbated by weight bearing or movement; it markedly impairs the functional capacity and daily functions of patients (5). The pathogenesis of BCP involves a complex mixture of tumor cells, bone cells, inflammatory microenvironment and the neuronal tissue (6). Therefore, research on the mechanisms of BCP may be useful for pain management.

Neuroinflammation in the spinal cord plays a pivotal role in the pathogenesis and maintenance of chronic pain, and is characterized by the infiltration of leukocytes, the activation of glial cells, and the production/secretion of pro-inflammatory cytokines and chemokines (7,8). Increased spinal inflammation has been reported in rodent models of several chronic pain, including inflammatory pain (9), neuropathic pain (10), chemotherapy-induced pain (11) and BCP (12,13). Research has provided evidence of neuroinflammation in the spinal cord of patients with chronic pain. Patients suffering from lumbar radiculopathy exhibit elevated levels of neuroinflammation marker translocator proteins in the spinal cord (14). A previous study demonstrated that the autopsy of spinal cord tissue from a patient with longstanding complex regional pain syndrome revealed the activation of astrocytic and microglial cells (15). It has been demonstrated that in patients positive for human immunodeficiency virus who suffer from chronic pain,

the levels of the pro-inflammatory cytokines, tumor necrosis factor α (TNF-α) and interleukin (IL)-1β, and the astrocytic markers, glial fibrillary acidic protein (GFAP) and S100β, are markedly increased in the spinal dorsal horn (16). The pharmacological inhibition of glial activation and pro-inflammatory cytokine release has been shown to exert an anti-nociceptive effect in animals (17). Of note, it has been shown that patients with spinal cord injury on an anti-inflammatory diet exhibit a decreased expression of interleukin (IL)-1β and IL-6, and an attenuation of sensory neuropathic pain (18). Electroacupuncture has also been found to exert a therapeutic effect on inflammatory pain by suppressing the expression of IL-1β and TNF-α (19). Oxidative stress in the spinal cord is a key contributor to neuroinflammation and neuropathic pain. A previous study demonstrated that the intrathecal injection of the reactive oxygen species (ROS) donor, tert-butyl hydroperoxide, led to transient hyperalgesia. However, systemic or intrathecal post-treatment with ROS scavengers significantly reduced hyperalgesia in a mouse model of capsaicin-induced pain (20). Glutathione also exerts an analgesic effect in models of neuropathic pain by reducing the ROS content and increasing the expression of antioxidant enzymes (21). In a a previous study, in rats with cancer-induced bone pain, the inhibition of the oxidative stress response and the elevation of the activity of the antioxidant enzyme, superoxide dismutase (SOD), reduced the pain sensitivity of rats (22). Increased levels of oxidative stress activate a variety of transcription factors in inflammatory pathways and trigger the inflammatory response (23). Thus, targeting spinal oxidative stress and inflammation may be a potential therapeutic strategy for neuropathic pain.

The phosphatidylinositol 3-kinase (PI3K)/protein kinase B (Akt) pathway participates in inflammatory cellular responses, mediates neuropathic pain and functions as a novel therapeutic target for inflammation-related diseases (24). LY294002, an inhibitor of PI3K, has been shown to alleviate endometriosis-associated sciatic nerve pain by inhibiting the PI3K/Akt/mammalian target of rapamycin signaling pathway (25). In a rat model of chronic constriction injury (CCI), the intrathecal injection of LY294002 was found to significantly block CCI-increased Akt phosphorylation and attenuate mechanical allodynia (26). In another study, in a rat model of BCP-morphine tolerance, the levels of phosphorylated (p-)PI3K, Akt and JNK1/2 were upregulated in the L4-6 spinal dorsal horn; however, the intrathecal injection of LY294002 decreased the phosphorylation levels of these proteins and attenuated the development of morphine tolerance (27).

In the present study, to investigate the effects of LY294002 on BCP and explore the underlying mechanisms, rats with BCP were intrathecally injected with LY294002 and the pain behaviors, motor ability, spinal inflammation and mitochondrial function were detected. The present study provides experimental data which may prove to be useful in alleviating BCP.

Materials and methods

Animals. A total of 36 male Sprague-Dawley (SD) rats, weighing 180-200 g (6-8 weeks old), were purchased from the Hubei Province Experimental Animal Center (Wuhan, China). All animals were housed in a temperature-controlled environment (22±1˚C) and 55±5% humidity with a 12-h light/dark cycle with *ad libitum* access to food and water. All procedures were conducted in accordance with the Chinese National Guidelines for the ethical review of animal welfare (GB/T 35892-2018) and approved by the Ethics Committee of Hubei University of Science and Technology (approval number 2020-01-900). The rats were allowed to acclimatize to their environment for 5 days prior to the start of the experiments. A total of 36 rats were randomly divided into four groups as follows: The sham-operated (sham), LY294002, BCP and BCP + LY294002 group, with 9 rats in each group.

Cells and cell culture. MRMT-1 rat breast cancer cells (cat. no. RCB2860; Jennio Biotech Co., Ltd.) were cultured in RPMI-1640 medium (Gibco; Thermo Fisher Scientific, Inc.) containing 10% fetal bovine serum (Gibco; Thermo Fisher Scientific, Inc.), 50 U/ml penicillin and 50 μg/ml streptomycin (Gibco; Thermo Fisher Scientific, Inc.) at 37˚C with 5% carbon dioxide. Rat glioma cells (C6) (cat. no. CBP60888; Jennio Biotech Co., Ltd.) were cultured in DMEM (Gibco; Thermo Fisher Scientific, Inc.) with 10% fetal bovine serum, 50 U/ml penicillin and 50 μg/ml streptomycin at 37˚C with 5% carbon dioxide.

Establishment of rat model of BCP and drug administration. To establish the rat model of BCP, MRMT-1 cells were collected and resuspended in Hank's balance salt solution (HBSS) (cat. no. 14170146; Gibco; Thermo Fisher Scientific, Inc.) and kept on ice until use. The rats were anaesthetized with pentobarbital sodium (50 mg/kg, intraperitoneal injection). The left hind limb was disinfected with 75% ethanol and $5.0x10^5$ MRMT-1 cells in HBSS were slowly injected into the intramedullary space of bones of the rats. The rats in the sham group were injected with an equivalent volume of the vehicle (HBSS). After 14 days of modeling, an intrathecal injection was administered using a 25-μl microsyringe, which was inserted into the intervertebral space of the rats between L5 and L6 vertebrae. The PI3K inhibitor, LY294002 (Selleck Chemicals), was dissolved in DMSO, and diluted with 0.9% NaCl (v/v 1:1) prior to use. The rats in the LY294002 and BCP + LY294002 groups were intrathecally injected with 10 μl LY294002 (1.5 mg/kg). The rats in the sham and BCP groups received an intrathecal injection of the same volume of the vehicle.

Bone X-ray and histological analysis. A roentgenograph of the left tibia was performed on the 14th day following the inoculation of the MRMT-1 cells. On day 14, 3 rats in each group were euthanized with an overdose of pentobarbital sodium (150 mg/kg) by intraperitoneal injection, the left tibiae were collected and fixed in 4% paraformaldehyde for 24 h, decalcified in 10% EDTA (Gibco; Thermo Fisher Scientific, Inc.) solution. The bone tissue was dehydrated and embedded in paraffin, and cut into 4-μm-thick sections using a microtome (Thermo Fisher Scientific, Inc.). The bone sections were then dewaxed and stained with hematoxylin and eosin (H&E) (Beyotime Institute of Biotechnology). Briefly, the sections were dyed with hematoxylin solution for 3 min and washed with tap water for 10 sec. The sections were stained with eosin for 3 min and washed with tap water for 10 sec. The dehydration

and transparent treatment were conducted by putting the slices into 80% ethanol (5 min), 90% ethanol (5 min), 95% ethanol (5 min), 100% ethanol (5 min, two times), xylene (5 min, times). The temperature used for all these procedures was 25˚C. Images were obtained using a microscope (Olympus IX73; Olympus Corporation).

Paw withdrawal threshold (PWT) test. The rats were placed in a 30x30x30 cm plexiglass chamber and were allowed to acclimatize to their environment for at least 30 min prior to the start of the behavioral experiments. von Frey filaments (Stoelting Co.; ranging from 0.4 to 26 g) were used by stimulating the left hind paws of the rats. Briefly, the filaments were pressed vertically against the plantar surfaces until the filaments were bent and held for 6-8 sec. Under this condition, a brisk withdrawal and paw flinching was considered a positive response. Once a positive response occurred, the von Frey filament with the next lower force was applied, and whenever a negative response occurred, the filament with the next higher force was applied. The pattern of positive and negative withdrawal response was used to determine the PWT.

Flinching number analysis. The rats were placed in a 30x30x30 cm plexiglass chamber and were allowed to acclimatize to their environment for at least 30 min prior to the start of the experiment. The number of flinches was recorded and counted for 5 min and repeated three times (28).

Rotarod test. An accelerating rotarod (ZS-RDM, Beijing Zhongshi Dichuang Science and Technology Development Co., Ltd.) was used to assess the motor coordination and balance of the animals. At 3 days prior to the start of the experiment, the animals received acclimatization training at a fixed speed of 4 r/min for 10 min repeating three times with 10-min intervals. At the beginning of experiment, the rotation speed was fixed at 10 r/min for 10 sec and then accelerated for 10 sec. Subsequently, the rod was working at a speed of 20 r/min for 30 sec and then accelerated for 10 sec. The movement was continuously carried out for 10 min, repeating three times with an interval of 10 min. The latency of the rats to fall was recorded.

Western blot analysis. Following 12 h of LY294002 and vehicle administration, another 3 rats from each group were euthanized by an overdose of pentobarbital sodium (150 mg/kg) by intraperitoneal injection and then subjected to decapitation. The spinal cord (L4-L6) was collected into ice-cold RIPA lysis buffer (Beyotime Institute of Biotechnology) containing a cocktail of protease inhibitors, homogenized on ice, and centrifugated at 12,000 x g, 4˚C for 15 min. The supernatant was collected and the protein concentration was measured using a BCA kit (Beyotime Institute of Biotechnology). Equal amounts of protein samples (35 μg) were separated by SDS-polyacrylamide gel (8-12%) electrophoresis, and electrically transferred onto PVDF membranes (MilliporeSigma). The membranes were then blocked with QuickBlock™ blocking buffer (Beyotime Institute of Biotechnology) at 25˚C for 1.5 h and incubated with the proper primary antibodies overnight at 4˚C. The following antibodies were used: IL-1β (1:1,000; cat. no. AF5103; Affinity Biosciences), TNF-α (1:1,000; cat. no. AF7014; Affinity Biosciences), GFAP (1:1,000; cat. no. BF0345; Affinity Biosciences), p-Akt (1:500; cat. no. AP1259; ABclonal Biotech Co., Ltd.), Akt (1:1,000; cat. no. A20799; ABclonal Biotech Co., Ltd.), nuclear factor (NF)-κB (1:1,000; cat. no. BF8005; Affinity Biosciences), BAX (1:1,000; cat. no. A20227; ABclonal Biotech Co., Ltd.), NADH:ubiquinone oxidoreductase subunit B11 (NDUFB11; 1:1,000; cat. no. A15617; ABclonal Biotech Co., Ltd.), dihydroorotate dehydrogenase (DHODH; 1:1,000; cat. no. A6899; ABclonal Biotech Co., Ltd.) and β-actin (1:50,000; cat. no. AC026; ABclonal Biotech Co., Ltd.). Following incubation (25˚C, 1 h) with goat anti-rabbit IgG (H + L)-HRP (1:10,000; cat. no. AS014; ABclonal Biotech Co., Ltd.) or goat anti-mouse IgG (H + L)-HRP (1:10,000; cat. no. AS003; ABclonal Biotech Co., Ltd.) secondary antibodies, the membranes were visualized with iBright 1500 (Invitrogen; Thermo Fisher Scientific, Inc.). The bands of target protein were analyzed using ImageJ 1.48v software (National Institutes of Health).

Immunofluorescence assay. Following treatment with LY294002 for 12 h, another 3 rats from each group were deeply anesthetized and myocardial perfused with 0.9% NaCl containing heparin, and subsequently switched perfusate to 4% polyformaldehyde. Following perfusion, the spinal cord was collected and fixed in 4% paraformaldehyde for 24 h, dehydrated, embedded in paraffin, and cut into 4-μm-thick sections using a microtome (Thermo Fisher Scientific, Inc.). The spinal cord sections were dewaxed, boiled at 95˚C in antigen repair solution (Beyotime Institute of Biotechnology) for 15 min, cooled naturally to normal temperature, incubated with 3% H_2O_2 solution (Guangdong Hengjian Pharmaceutical Co., Ltd.) for 10 min, blocked with immunofluorescence blocking solution (Beyotime Institute of Biotechnology) at 25˚C for 1 h and subsequently incubated with primary antibodies at 4˚C for 24 h. Including IL-1β (1:100; cat. no. AF5103; Affinity Biosciences), GFAP (1:100; cat. no. BF0345; Affinity Biosciences), PI3K (1:100; cat. no. AF6241; Affinity Biosciences), p-Akt (1:100; cat. no. AP1259; ABclonal Biotech Co., Ltd.), NDUFB11 (1:100; cat. no. A15617; ABclonal Biotech Co., Ltd.) and BAX (1:100; cat. no. A20227; ABclonal Biotech Co., Ltd.), and goat-rabbit IgG H&L (FITC) (1:500; cat. no. ab6717; Abcam) at 25˚C for 1 h. They were then mounted with antifade mounting medium (Beyotime Institute of Biotechnology). Images were acquired using a fluorescence microscope (Olympus Corporation). The intensity was analyzed using ImageJ 1.48v software (National Institutes of Health).

Transmission electron microscopy (TEM) assay. The morphology of the mitochondria in the spinal cord were confirmed using electron microscopy with negative staining. Briefly, the spinal cord tissues from another 3 rats from each group were isolated, cut into ~1 mm^3 cubes, fixed in 2.5% glutaraldehyde (Sigma-Aldrich Shanghai Trading Co., Ltd.) at 25˚C for 4 h and post-fixed with 1% osmium tetroxide (Electron Microscopy China) at 25˚C for 2 h. Ultrathin sections were post-stained with uranyl acetate (Electron Microscopy China) for 30 min and lead citrate (Electron Microscopy China) for 15 min and then examined using an

HC-1 transmission electron microscope (Hitachi Corporation) operating at 120 kV.

Detection of manganese SOD (Mn-SOD) activity. To detect the enzyme activity of Mn-SOD, the CuZn/Mn-SOD assay kit with WST-8 (cat. no. S0103; Beyotime Institute of Biotechnology) were used. Briefly, the spinal cords were homogenized in ice-cold phosphate-buffered saline (PBS) and centrifuged at 12,000 x g, 4˚C for 15 min. The supernatant was collected and incubated with Cu/Zn-SOD inhibitors for 1 h at 37˚C. After mixing with WST-8 enzyme working solution for 20 min at 37˚C, the absorbance value at $OD_{450\,nm}$ of each pore was measured. The Mn-SOD activity was expressed as units per milligram of total protein (U/mg protein).

Malondialdehyde (MDA) assay. The levels of MDA were measured using the MDA Assay kit (cat. no. S0131S; Beyotime Institute of Biotechnology). Briefly, the spinal cord tissues were lysis using ice-cold RIPA lysis buffer (Beyotime Institute of Biotechnology) and centrifuged at 12,000 x g, 4˚C for 15 min. The supernatant acquired was mixed with MDA working solution, heated at 95˚C for 15 min, and centrifugated at 1,000 x g, 25˚C for 10 min after cooling naturally to room temperature. The supernatant was collected and the absorbance was measured at 532 nm. The MDA levels were calculated according to the standard curve and expressed as μmol/mg protein.

Measurement of mitochondrial membrane potential (MMP). MMP was measured using a fluorescent probe JC-1 (Beyotime Institute of Biotechnology). The C6 cells were inoculated in the 24-well plate with sterilized coverslips, stimulated with IL-1β (5 ng/ml; Beyotime Institute of Biotechnology) for 30 min and incubated with 1 μM LY294002 at 37˚C for 24 h. The cells were then cultured with 200 μl JC-1 for 20 min at 37˚C in the dark, and the fluorescence intensity was detected using a fluorescence microscope (Olympus Corporation). Mitochondrial uncoupler carbonyl cyanide 3-chlorophenylhydrazone (CCCP, 10 μM) treatment was used as positive control, since it disrupts mitochondrial integrity and induced the loss of MMP (29).

Measurement of mitochondrial ROS generation. MitoSOX Red mitochondrial superoxide indicator (Thermo Fisher Scientific, Inc.), a novel fluorogenic dye, was used to detect mitochondrial superoxide in C6 cells. Briefly, the cells were inoculated in the 24-well plate with sterilized coverslips, stimulated with IL-1β, incubated with LY294002, subsequently incubated with 5 μM MitoSOX Red (Molecular Probes, Thermo Fisher Scientific, Inc.) in the dark at 37˚C for 10 min and detected under a fluorescence microscope (Olympus Corporation).

Statistical analysis. All statistical analyses were performed using the SPSS 26 software package (IBM Corp.). One-way analysis of variance (one-way ANOVA) was used to evaluate the differences between the experimental groups followed by Bonferroni post hoc tests. The results of the behavioral tests are presented as the mean ± SEM. Other experiment data are presented as the mean ± SD. $P<0.05$ was considered to indicate a statistically significant difference.

Results

Intratibial inoculation of tumor cells induces bone destruction, hyperalgesia and motor impairment in rats. After 5 days of acclimatization, the rats were inoculated with MRMT-1 cells to establish the model of BCP. To verify the establishment of the BCP model, X-rays, H&E staining and behavioral tests were performed (Fig. 1A). Radiographs of the rat tibiae were obtained on day 14 post-surgery and revealed notable bone destruction, particularly at the proximal epiphysis. Fewer radiolucent lesions in the tibiae were observed in the rats in the sham group (Fig. 1B). Moreover, the histological analysis of the tibiae from rats with BCP revealed that there was an increased cell infiltration in the bone marrow spaces and a loss of normal bone structure, whereas bone loss was not evident in the sham group (Fig. 1C). Pain behavioral testing revealed that there were no significant differences in mechanical withdrawal, the number of spontaneous flinches and latency to fall between the rats in the sham and BCP groups prior to cancer cell inoculation (Fig. 1D-F). Following the intratibial inoculation of MRMT-1 cells, mechanical allodynia, spontaneous flinching behavior and the impairment of motor functions developed on day 4 and persisted for at least 14 days. By contrast, no marked changes were observed in the PWT value, the number of spontaneous flinches and the latency to fall in the rats in the sham group following surgery. Taken together, these results suggested that the inoculation of MRMT-1 cells induced bone destruction, pain hypersensitivity and motor impairment in the rats.

LY294002 treatment alleviates pain hypersensitivity and motor impairment. To confirm the effects of the PI3K/Akt pathway on pain behaviors, the expression and localization of PI3K and Akt in the spinal cords of the rats were analyzed, and the pain behavior and motor performance were further assessed following treatment with the PI3K inhibitor, LY294002. Immunofluorescence analysis revealed the enhanced fluorescence signals of PI3K and p-Akt in the spinal dorsal horn of rats with BCP (Fig. 2A-C). Western blot analysis also revealed an increase in the level of p-Akt in the rats with BCP (Fig. 2D and E). Upon treatment with LY294002, the levels of PI3K and p-Akt were significantly decreased in the spinal cords of rats with BCP, as detected using immunofluorescence and western blot analysis. However, LY294002 had no effect on the PI3K/Akt pathway in the spinal cords of the rats in the sham group (Fig. 2A-E). Subsequently, behavioral tests were performed following treatment with LY294002. The results indicated that the intrathecal injection of LY294002 significantly increased the PWT values (Fig. 2F), decreased the numbers of spontaneous flinches (Fig. 2G) and increased the latency to fall (Fig. 2H) in the rats with BCP. However, there were no significant changes between the rats in the sham and LY294002 groups (Fig. 2F-H). These results indicated that LY294002 exerted an inhibitory effect on mechanical pain and spontaneous pain, and a beneficial effect on the motor impairment of rats with BCP.

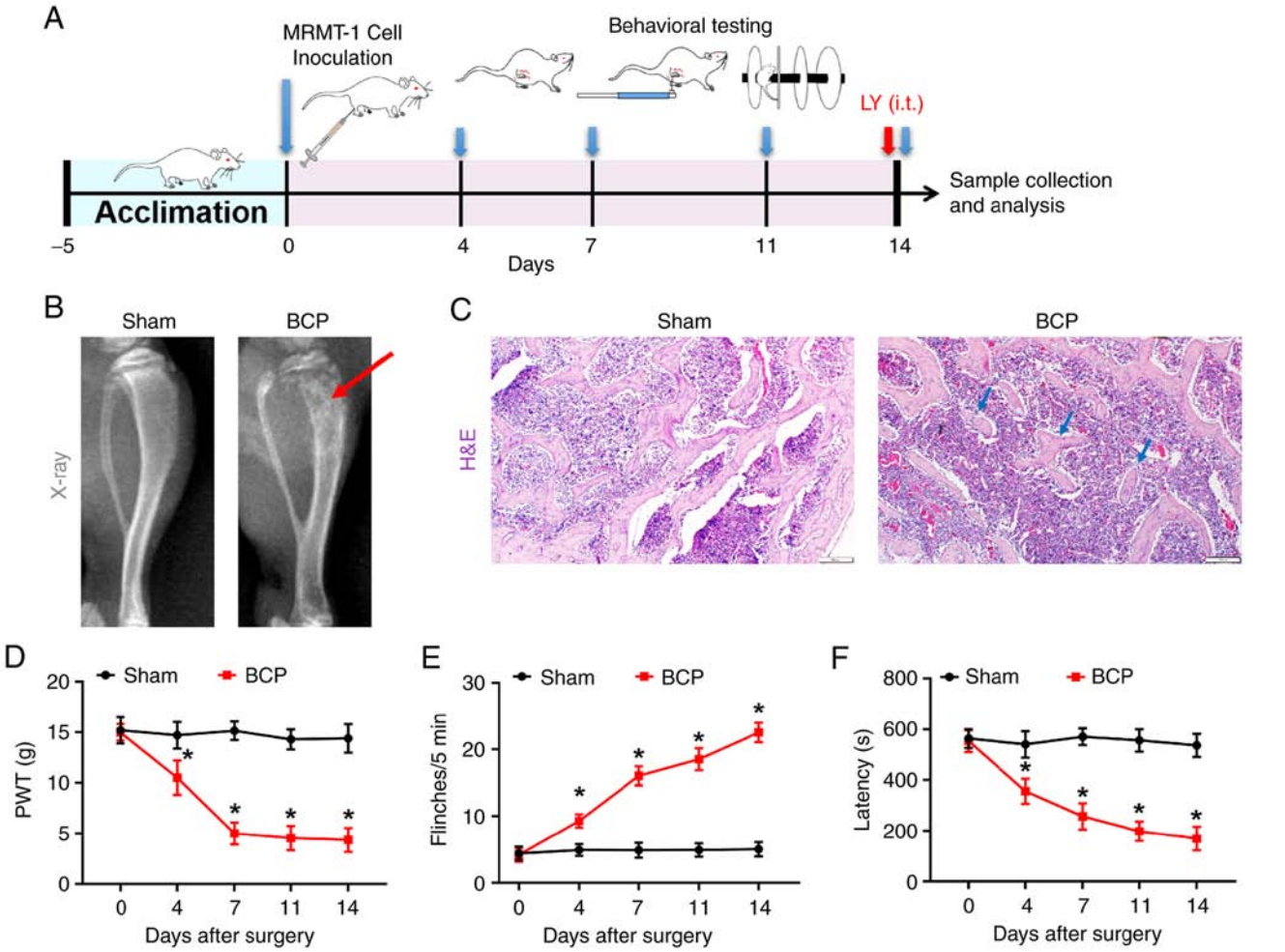

Figure 1. Establishment of the rat model of BCP and the assessment of bone morphology, pain and locomotor behaviors in rats. (A) Schematic diagram of the study design: Inoculation of MRMT-1 cells to establish BCP in rats following acclimation. The behavioral tests were performed on days 0, 4, 7, 11 and 14 post-surgery. Tissue samples were then collected for morphological and protein expression analyses. (B) Radiographs of the tibiae from the rats in the sham and BCP groups on day 14 after the MRMT-1 cell inoculation (n=5). The red arrow indicates the structural destruction in rats with BCP. (C) Hematoxylin and eosin staining of tibial sections revealed bone loss and bone destruction on day 14 following MRMT-1 cell inoculation (n=5). The blue arrows indicate the discontinuous trabecular structure. Scale bars, 100 μm. (D) The PWT of rats from the sham and BCP group in response to von Frey filaments at the indicated time points (days 0, 4, 7, 11 and 14 following inoculation). (E) The number of spontaneous flinches in a 5-min period of the sham and BCP group rats. (F) The latency to fall of the sham and BCP group rats in the rotarod test. The data of behavioral tests are presented as the mean ± SEM from at least 9 rats in each group. *P<0.05 vs. the sham group. BCP, bone cancer pain; PWT, paw withdrawal threshold.

LY294002 treatment inhibits astrocytic activation and the inflammatory response in rats with BCP. The robust astrocyte activation and the release of IL-1β from activated astrocytes are closely related to chronic pain (30). To identify the activation of astrocytes and spinal inflammation, immunofluorescence staining was performed for GFAP, a marker of abnormal activation and the proliferation of astrocytes (an astrocytic marker) (31) and IL-1β. The results revealed that compared with the sham group, the fluorescence intensities of GFAP and IL-1β in the spinal dorsal horns of rats with BCP were significantly enhanced (Fig. 3A-C). Western blot analysis revealed the increased expression levels of GFAP and IL-1β in rats with BCP. In addition to IL-1β, upregulated TNF-α protein levels were also detected in the rats with BCP (Fig. 3D and E). Treatment with LY294002 significantly reduced the fluorescence intensities of GFAP and IL-1β, and decreased the protein levels of GFAP, IL-1β and TNF-α in the rats with BCP, and exerted inhibitory effects on both astrocyte activation and pro-inflammatory cytokine expression. However, no significant changes were detected in the levels of GFAP, IL-1β and TNF-α in the rats in the sham and LY294002 groups (Fig. 3). Since the nuclear transcription factor NF-κB mediated the expression of pro-inflammatory cytokines, the expression of NF-κB was further detected. The results revealed that LY294002 treatment also reduced the expression of NF-κB in the rats with BCP (Fig. 3D and E). These data indicated that LY294002 treatment inhibited the spinal astrocytic activation and inflammatory response in rats with BCP.

LY294002 treatment blocks mitochondrial dysfunction in rats with BCP. The PI3K/Akt pathway regulates mitochondrial function and dynamics by inhibiting BAX translocation from the cytoplasm to the mitochondria (32); therefore, the BAX expression level was analyzed in the present study. In contrast to the sham group, the fluorescence intensity and protein level of BAX were significantly upregulated in the BCP group, while LY294002 treatment reduced both the BAX fluorescence intensity and the protein level (Fig. 4A and B). Second,

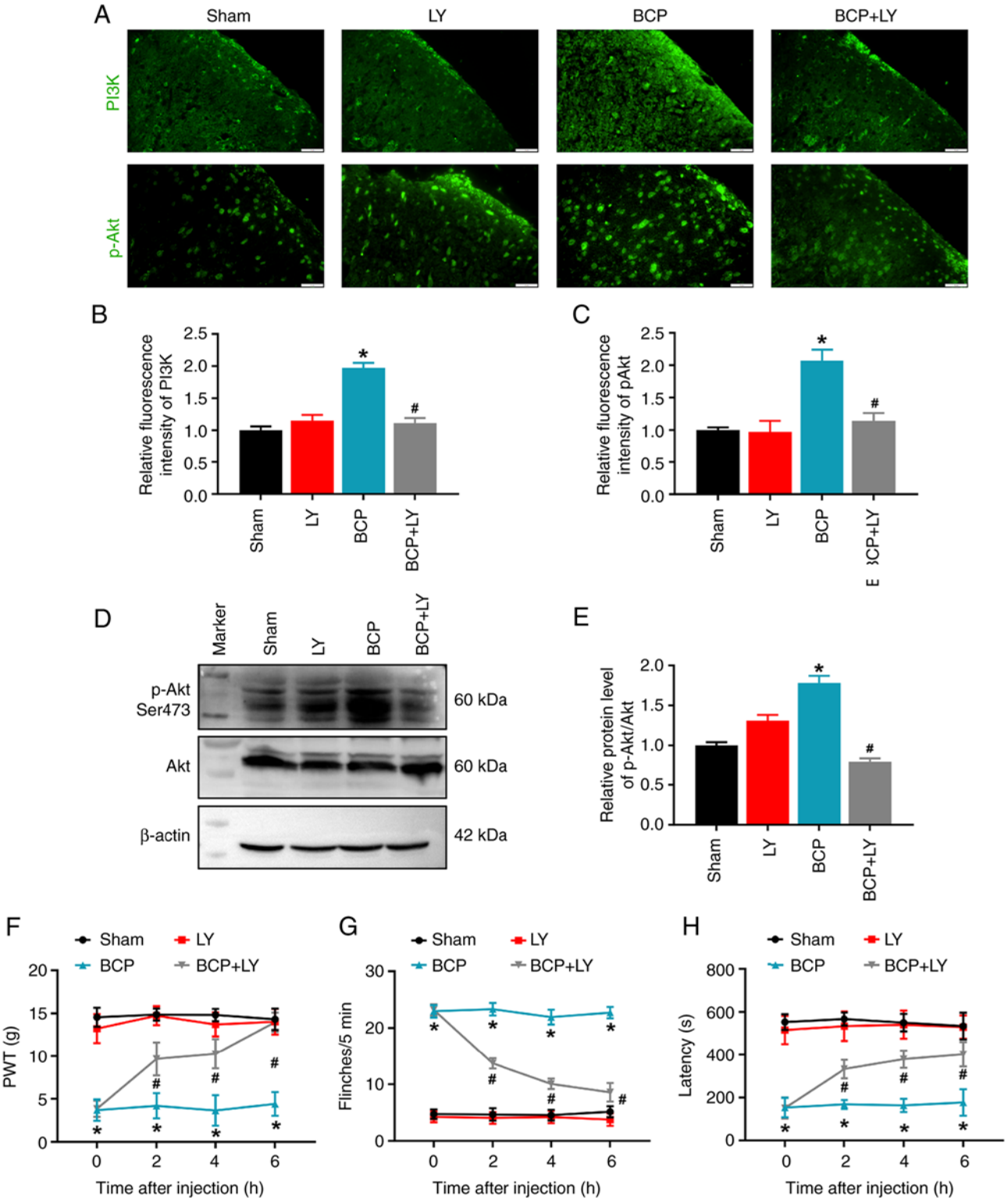

Figure 2. Effects of LY294002 on the PI3K/Akt signaling pathway and behaviors of rats with BCP. (A) Immunofluorescence staining of PI3K and p-Akt in the spinal cord sections from the rats in the sham, LY294002-treated sham, BCP and LY294002-treated BCP groups. Scale bars, 20 μm. (B and C) Quantitative analysis of the fluorescence intensity of PI3K and p-Akt. Data are expressed as the mean ± SD (n=3). (D) The protein levels of p-Akt (Ser473) and total Akt in lumbar spinal cord were detected using western blot analysis. (E) Quantification of Akt phosphorylation. Data are expressed as the ratio of p-Akt/total Akt and each bar represents the mean ± SD (n=3). Comparison of (F) PWT value, (G) numbers of flinches, and (H) latency to fall in the sham, LY294002, BCP and BCP + LY294002 groups. Data are expressed as the mean ± SEM (n=9). *P<0.05 vs. sham group, $^{\#}$P<0.05 vs. BCP group. BCP, bone cancer pain; PWT, paw withdrawal threshold.

the mitochondrial morphology was observed with TEM. The TEM images revealed that the mitochondria in the sham group contained a whole inner membrane, outer membrane and cristae in an oval shape. However, in the BCP group, mitochondrial cristae were lost, and the mitochondrial size and perimeter were decreased (Fig. 4C). Subsequently, the changes

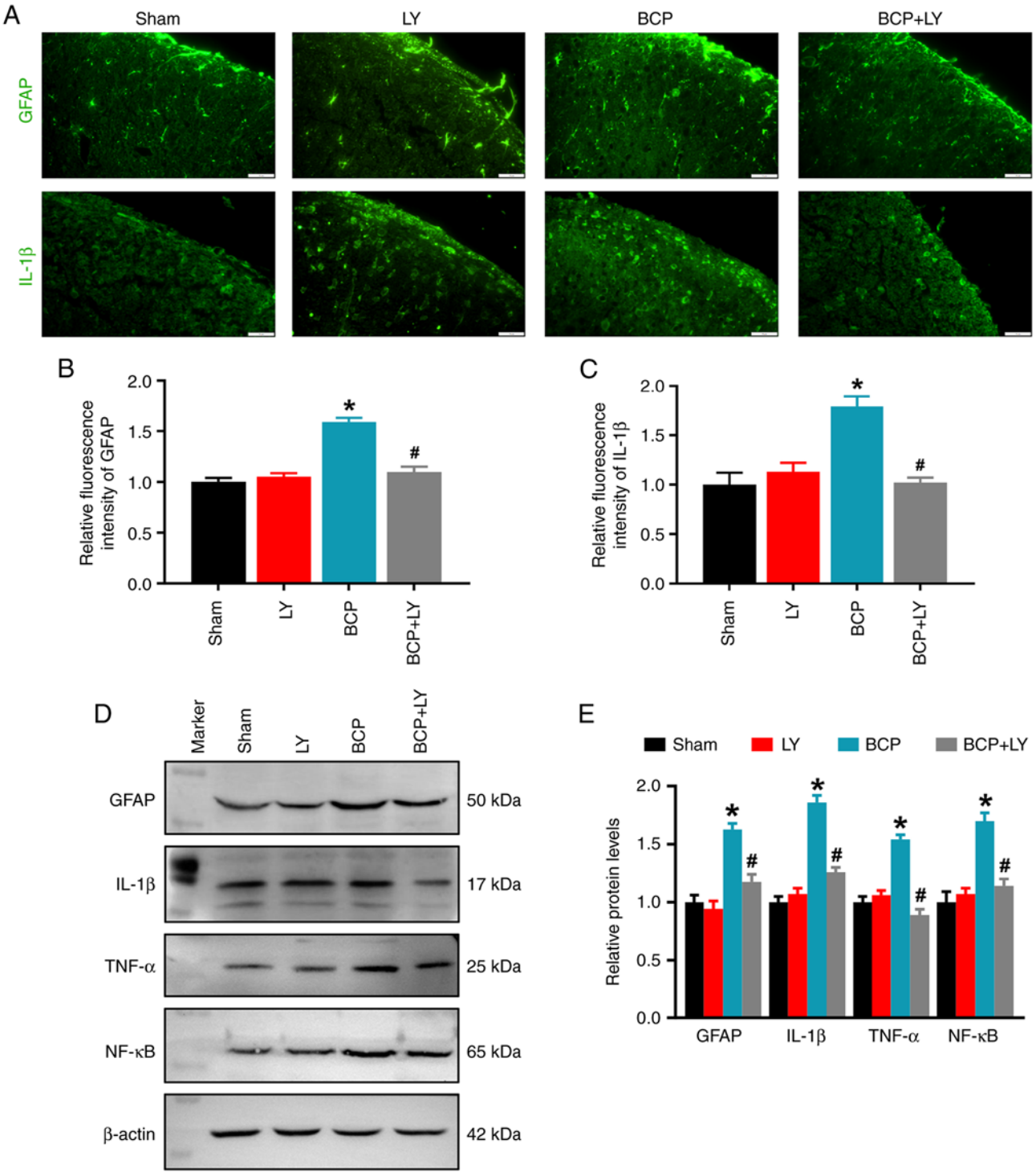

Figure 3. Effects of LY294002 on spinal GFAP, IL-1β, TNF-α and NF-κB protein levels. (A) Immunofluorescence staining of GFAP and IL-1β on spinal cord sections from the sham, LY294002-treated sham, BCP and LY294002-treated BCP group rats. Scale bars, 20 μm. (B and C) Quantitative analysis of GFAP and IL-1β fluorescence intensity. Data are expressed as the mean ± SD (n=3). (D) Western blot analysis of GFAP, IL-1β, TNF-α and NF-κB protein expression in the lumbar spinal cord. (E) Quantification of the protein levels by relative greyscale analysis. Data are expressed as mean ± SD (n=3). *P<0.05 vs. sham group, $^{\#}$P<0.05 vs. BCP group. BCP, bone cancer pain; GFAP, glial fibrillary acidic protein; IL, interleukin; TNF-α, tumor necrosis factor α.

in mitochondrial function were determined by determining the activity of the Mn-SOD enzyme and the levels of mitochondrial proteins. As shown in Fig. 4D, Mn-SOD activity, the primary antioxidant enzyme in the mitochondria, markedly decreased in the spinal cords of rats with BCP. LY294002 treatment remarkably increased the Mn-SOD activity of BCP rats (Fig. 4D). Apart from this antioxidant, the levels of the marker of oxidative stress, MDA, were analyzed; an increase in the MDA level was observed in the spinal cords of rats in the BCP group. LY294002 treatment increased Mn-SOD activity and reduced the MDA level in the rats with BCP (Fig. 4D and E). Subsequently, the expression levels of the mitochondrial protein, NDUFB11 (a component of mitochondrial complex I) and DHODH (an antioxidant which inhibits lipid peroxidation

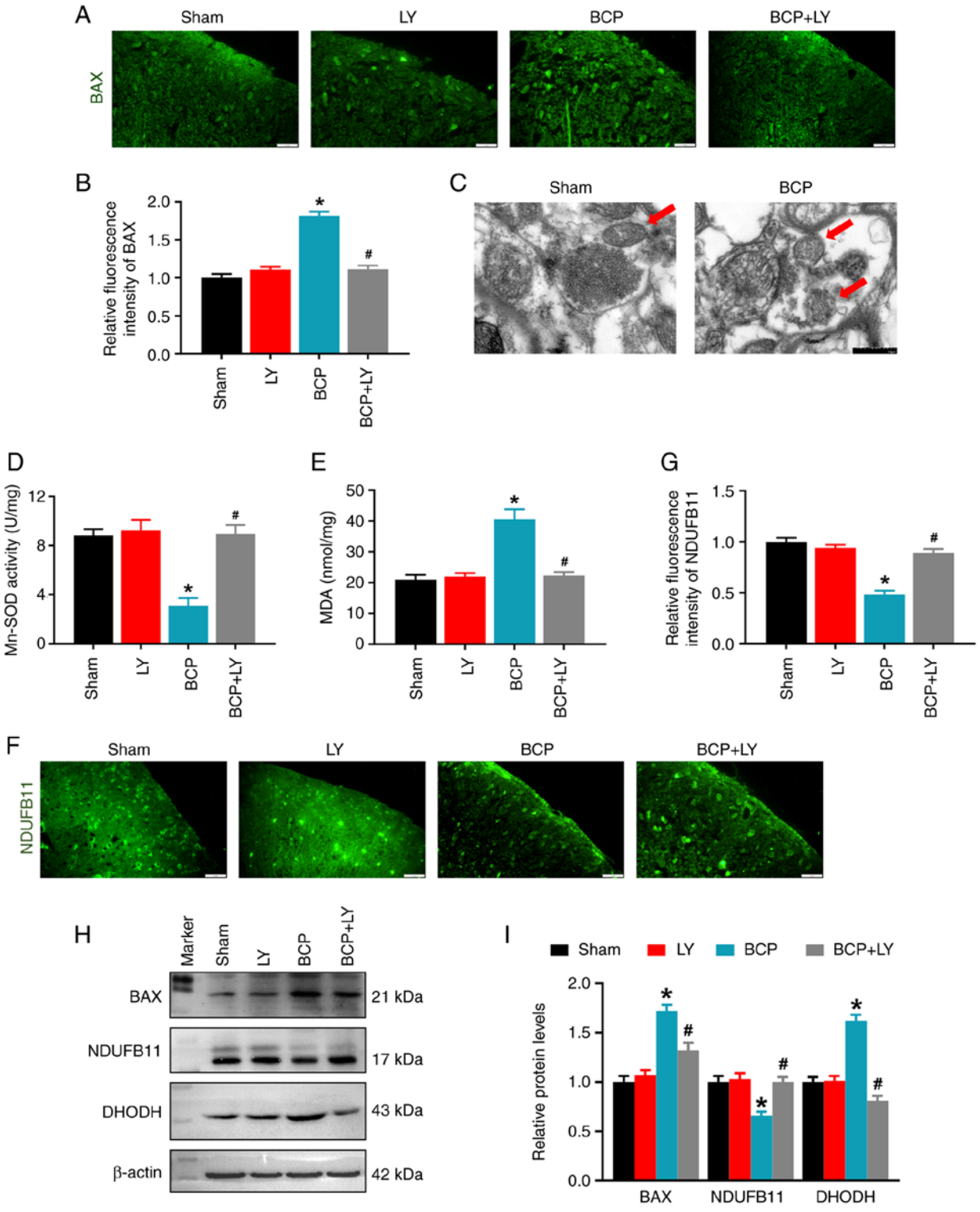

Figure 4. Effects of LY294002 on the spinal BAX level and mitochondrial morphology and function. (A) Immunofluorescence staining of BAX on spinal cord sections. Scale bars, 20 μm. (B) Quantitative analysis of BAX fluorescence intensity. Data are expressed as the mean ± SD (n=3). (C) Representative transmission microscopy images of mitochondria in the spinal cord of rats in the sham and BCP groups. Scale bars, 0.5 μm. The red arrows indicate the mitochondria. (D) Changes in Mn-SOD activity detected using the Mn-SOD Assay kit. Data are expressed as the mean ± SD (n=3). (E) Changes in the MDA level of the spinal cord. Data are expressed as the mean ± SD (n=3). (F) Immunofluorescence staining of NDUFB11 on spinal cord sections. Scale bars, 20 μm. (G) Quantitative analysis of NDUFB11 fluorescence intensity. Data are expressed as the mean ± SD (n=3). (H) The protein levels of BAX, NDUFB11 and DHODH in lumbar spinal cord were detected using western blot analysis. (I) Quantification of the protein level by relative greyscale analysis. Data are expressed as the mean ± SD (n=3). *P<0.05 vs. sham group, $^{\#}$P<0.05 vs. BCP group. BCP, bone cancer pain; Mn-SOD, manganese superoxide dismutase; MDA, malondialdehyde; NDUFB11, NADH:ubiquinone oxidoreductase subunit B11; DHODH, dihydroorotate dehydrogenase.

in the mitochondria) were examined using immunofluorescence and western blot analysis. The fluorescence intensity of NDUFB11 in the spinal dorsal horn was markedly decreased in the BCP group, and the intensity was increased following

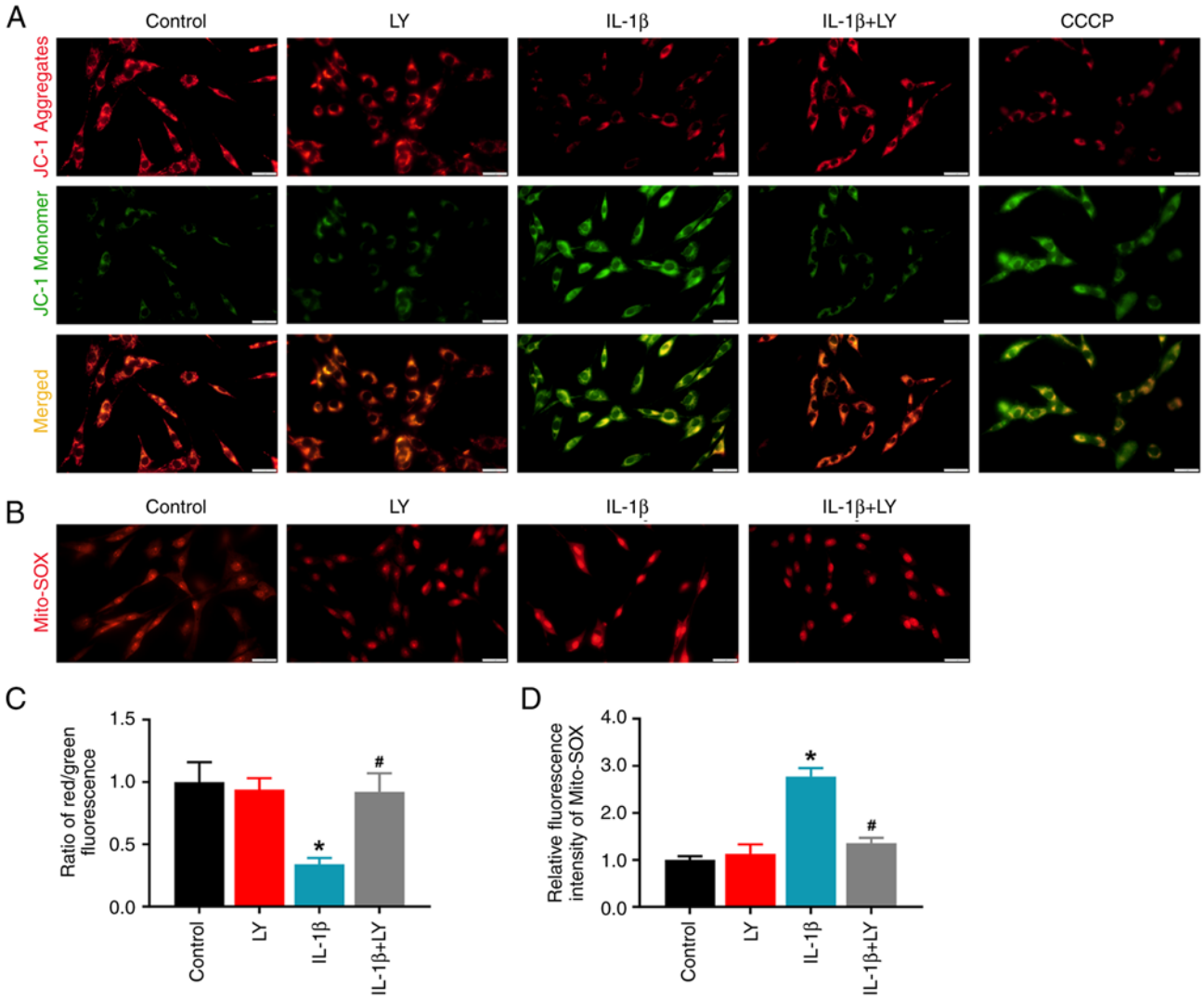

Figure 5. Effects of LY294002 on mitochondrial function in IL-1β-stimulated C6 cells. (A) Detection of the mitochondrial membrane potential in the control, LY294002, IL-1β, and IL-1β + LY294002 groups by labeling with the JC-1. CCCP-treated cells were used as the positive control. (B) Detection of mitochondrial ROS by labeling with MitoSOX. Quantitative fluorescence intensity of (C) JC-1 and (D) Mito-ROS. Data are expressed as the mean ± SD. *P<0.05 vs. control group, #P<0.05 vs. IL-1β group. IL, interleukin; CCCP, 3-chlorophenylhydrazone.

treatment with LY294002 (Fig. 4F and G). Western blot analysis revealed that the expression level of spinal NDUFB11 was decreased in the rats with BCP and LY294002 treatment upregulated the NDUFB11 expression level (Fig. 4H and I). By contrast, the relative level of DHODH was increased in the BCP group and LY294002 treatment decreased the DHODH protein level (Fig. 4H and I). These results indicated that LY294002 treatment reduced oxidative stress and restored mitochondrial function in rats with BCP.

LY294002 treatment improves mitochondrial function in C6 cells. To verify the effects of LY294002 on mitochondrial function, changes in MMP and mitochondrial ROS were detected using JC-1 and the MitoSOX red indicator. For JC-1 analysis, the monomeric green form indicates a lower MMP, while red aggregates indicate a higher MMP. MitoSOX red indicators specifically bind with mitochondrial superoxide. As shown in Fig. 5, IL-1β stimulation in C6 cells induced a lower MMP. LY294002 treatment restored the MMP in the IL-1β + LY group (Fig. 5A and C). IL-1β stimulation enhanced Mito-ROS intensity, and LY294002 treatment markedly reduced the mitochondrial ROS level in the IL-1β + LY294002 group (Fig. 5B and D). However, LY294002 had no effect on the control cells.

Discussion

Cancer metastases is the cause of 90% of cancer-related deaths, and bones are the third most frequent target sites of metastases after the lungs and liver (33). Breast cancer, as the most common type of cancer, tends to spread to the bones more often than other parts of the body. Once cancer has spread to the bones, tumor cells growing in bone marrow induce osteolysis and bone destruction, injure the peripheral nerves and stimulate the inflammatory process (34). These reactions in the bone cause peripheral sensitization presenting as the activated pain signaling pathway and a lowered pain threshold (35). In the present study, MRMT-1 rat breast carcinoma cells were inoculated into the intramedullary space of rat tibiae and induced bone damage, pain hypersensitive and

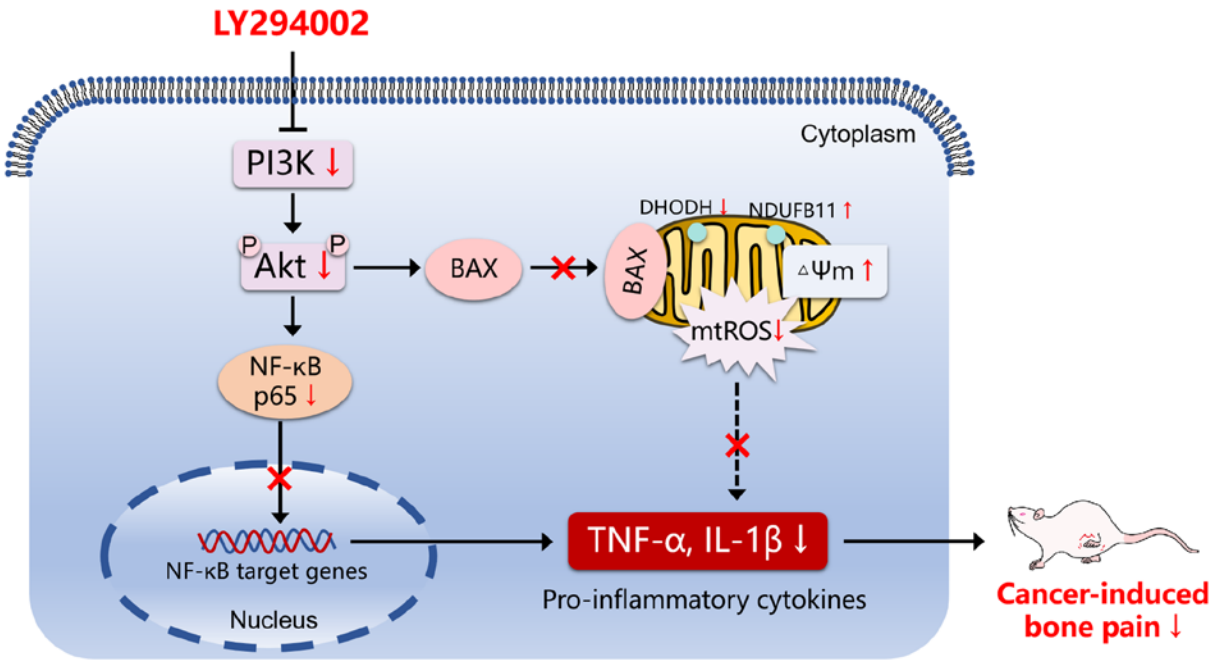

Figure 6. Schematic representation of the molecular mechanisms of PI3K inhibition and its effects on pain behaviors of rats with cancer-induced bone pain. IL, interleukin; TNF-α, tumor necrosis factor α; NDUFB11, NADH:ubiquinone oxidoreductase subunit B11; DHODH, dihydroorotate dehydrogenase; mtROS, mitochondrial reactive oxygen species.

motor disability. These symptoms indicated that the rat model of BCP was successfully established and suitable for research.

Peripheral noxious stimuli are conveyed to the spinal cord and are finally passed to numerous parts of the brain (36). During these processes, the spinal cord undergoes central sensitization and functions on pain maintenance (37). Therefore, spinal cord stimulation has been used to treat a variety of pain conditions and improve the quality of life of patients (38). Astrocytes in the spinal dorsal horn exhibit variable morphological and functional alterations, and stimulate pain hypersensitivity following peripheral nerve injury conditions (39). In the present study, astrocytes were activated and pro-inflammatory cytokine expression was increased in the spinal cords of rats with BCP, which were suppressed by treatment with the PI3K inhibitor, LY294002.

PI3Ks play a key role in the inflammatory response. The selective inhibition of PI3Ks offers a therapeutic opportunity for inflammatory pathologies (40). In the present study, LY294002 was used to treat rats with BCP and its inhibitory effects on inflammatory signal activation were observed. Several signal pathways are involved in the effects of PI3K/Akt signaling on spinal inflammation and pain. The inhibition of PI3Kα/δ/β plays a key role in the inflammatory response to damage and infection (41,42). PI3K/Akt inhibition by compound 8C and PIK-75 has been shown to markedly decrease the production and biological activity of pro-inflammatory cytokines, such as TNF-α and IL-6 in a NF-κB-dependent manner (43,44), which is considered the central mediator of inflammatory process by inducing the expression of various pro-inflammatory genes (45,46). In the present study, it was found that LY294002 treatment inhibited the activation of the PI3K/Akt signal pathway, and decreased the upregulated expression of NF-κB, TNF-α and IL-1β in the spinal cords of rats with BCP. Accordingly, LY294002 suppressed spinal inflammation via the PI3K/Akt/NF-κB pathway.

Mitochondrial cristae membranes contain a number of enzymes for electron transport chain (47) and oxidative phosphorylation (48). NDUFB11 is a relatively small integral membrane protein and is absolutely essential for the assembly of an active mitochondrial complex I of respiratory chain (49). The mitochondrial enzyme DHODH couples the respiratory chain to the de novo pyrimidine biosynthesis pathway (50), associates with the function of respiratory complexes II and III (51), and mediates ROS generation (52). Mitochondrial structure, distribution and function are dependent on energy demands. High energy demands and high rates of ATP production and consumption in the spinal dorsal horn drive mitochondrial destruction and dysfunction (53). The present study demonstrated that, in the spinal cords of rats with BCP, mitochondrial structure and function were damaged, exhibiting disappeared cristae, a decreased Mn-SOD activity, a reduced NDUFB11 expression, and an increased DHODH expression. Moreover, cell research has indicated that inflammation induced MMP deficiency and elevated mitochondrial ROS levels. The increased production of mitochondrial ROS triggers the activation of the NF-κB inflammatory pathway and promotes the synthesis of pro-inflammatory cytokines (54). BAX localizes largely in the cytoplasm, redistributes to the mitochondria in response to stimuli, triggers the release of cytochrome *c*, and consequently induces mitochondrial dysfunction (55). It has been reported that LY294002 treatment inhibits the PI3K/Akt pathway, suppresses BAX translocation to the mitochondria and reduces the release of mitochondrial ROS (56). The knockdown of DHODH has been shown to increase BAX expression (57). Herein, LY294002 treatment suppressed BAX and DHODH expression, increased NDUFB11 expression, elevated Mn-SOD activity, and reduced the mitochondrial and cellular ROS levels. Taken together, the inhibition of PI3K/Akt signaling by LY294002 restored mitochondrial function in rats with BCP.

In conclusion, the present study demonstrates that, in the process of BCP, the PI3K/Akt pathway is activated, mitochondrial dysfunction is induced, and the spinal inflammatory response is triggered. The inhibition of the PI3K/Akt pathway by LY294002 treatment alleviates BCP by suppressing BAX and DHODH activity, reducing the mitochondrial ROS level and consequently decreasing the NF-κB-mediated inflammatory signal in the spinal cord (Fig. 6).

Acknowledgements

Not applicable.

Funding

The present study was supported by the National Natural Science Foundation of China (grant nos. 81901149, 81971066 and 32100823), and the Hubei University of Science and Technology Program (grant nos. 2020TD02 and BK202116).

Availability of data and materials

The datasets generated and analyzed during the present study are available from the corresponding author on reasonable request.

Authors' contributions

All authors made a significant contribution to the study. HZ and MX conceived and designed the study, and drafted and edited the manuscript. JZ, YY, SZ, LY and LL performed the experiments, JD and QT collected and analyzed the data. HZ, MX, JD and QT critically revised the manuscript. All authors have read and approved the final manuscript. JZ and YY confirm the authenticity of all the raw data.

Ethics approval and consent to participate

All procedures involving animals were conducted in accordance with the Chinese National Guidelines for ethical review of animal welfare (GB/T 35892-2018) and approved by the Ethics Committee of Hubei University of Science and Technology (approval no. 2020-01-900).

Patient consent for publication

Not applicable.

Competing interests

The authors declare that they have no competing interests.

References

1. Zajączkowska R, Kocot-Kępska M, Leppert W and Wordliczek J: Bone pain in cancer patients: Mechanisms and current treatment. Int J Mol Sci 20: 6047, 2019.
2. Sung H, Ferlay J, Siegel RL, Laversanne M, Soerjomataram I, Jemal A and Bray F: Global cancer statistics 2020: GLOBOCAN estimates of incidence and mortality worldwide for 36 cancers in 185 countries. CA Cancer J Clin 71: 209-249, 2021.
3. Mercadante S: Malignant bone pain: Pathophysiology and treatment. Pain 69: 1-18, 1997.
4. Gallaway MS, Townsend JS, Shelby D and Puckett MC: Pain among cancer survivors. Prev Chronic Dis 17: E54, 2020.
5. Kane CM, Hoskin P and Bennett MI: Cancer induced bone pain. BMJ 350: h315, 2015.
6. Kapoor R, Saxena AK, Vasudev P, Sundriyal D and Kumar A: Cancer induced bone pain: Current management and future perspectives. Med Oncol 38: 134, 2021.
7. Vergne-Salle P and Bertin P: Chronic pain and neuroinflammation. Joint Bone Spine 88: 105222, 2021.
8. Ji RR, Xu ZZ and Gao YJ: Emerging targets in neuroinflammation-driven chronic pain. Nat Rev Drug Discov 13: 533-548, 2014.
9. Zhang S, Li Y and Tu Y: Lidocaine attenuates CFA-induced inflammatory pain in rats by regulating the MAPK/ERK/NF-κB signaling pathway. Exp Ther Med 21: 211, 2021.
10. Sommer C, Leinders M and Üçeyler N: Inflammation in the pathophysiology of neuropathic pain. Pain 159: 595-602, 2018.
11. Wahlman C, Doyle TM, Little JW, Luongo L, Janes K, Chen Z, Esposito E, Tosh DK, Cuzzocrea S, Jacobson KA and Salvemini D: Chemotherapy-induced pain is promoted by enhanced spinal adenosine kinase levels through astrocyte-dependent mechanisms. Pain 159: 1025-1034, 2018.
12. Zheng XQ, Wu YH, Huang JF and Wu AM: Neurophysiological mechanisms of cancer-induced bone pain. J Adv Res 35: 117-127, 2021.
13. Li MY, Ding JQ, Tang Q, Hao MM, Wang BH, Wu J, Yu LZ, Jiao M, Luo BH, Xie M and Zhu HL: SIRT1 activation by SRT1720 attenuates bone cancer pain via preventing Drp1-mediated mitochondrial fission. Biochim Biophys Acta Mol Basis Dis 1865: 587-598, 2019.
14. Albrecht DS, Ahmed SU, Kettner NW, Borra RJH, Cohen-Adad J, Deng H, Houle TT, Opalacz A, Roth SA, Melo MFV, *et al*: Neuroinflammation of the spinal cord and nerve roots in chronic radicular pain patients. Pain 159: 968-977, 2018.
15. Del VL, Schwartzman RJ and Alexander G: Spinal cord histopathological alterations in a patient with longstanding complex regional pain syndrome. Brain Behav Immun 23: 85-91, 2009.
16. Shi Y, Gelman BB, Lisinicchia JG and Tang SJ: Chronic-pain-associated astrocytic reaction in the spinal cord dorsal horn of human immunodeficiency virus-infected patients. J Neurosci 32: 10833-10840, 2012.
17. Liu B, Luo M, Meng D, Pan H, Shen H, Shen J, Yao M and Xu L: Tetrahydropalmatine exerts analgesic effects by promoting apoptosis and inhibiting the activation of glial cells in rats with inflammatory pain. Mol Pain 17: 17448069211042117, 2021.
18. Allison DJ, Thomas A, Beaudry K and Ditor DS: Targeting inflammation as a treatment modality for neuropathic pain in spinal cord injury: A randomized clinical trial. J Neuroinflammation 13: 152, 2016.
19. Yu ML, Wei RD, Zhang T, Wang JM, Cheng Y, Qin FF, Fu SP, Lu ZG and Lu SF: Electroacupuncture relieves pain and attenuates inflammation progression through inducing IL-10 Production in CFA-Induced mice. Inflammation 43: 1233-1245, 2020.
20. Schwartz ES, Lee I, Chung K and Mo Chung J: Oxidative stress in the spinal cord is an important contributor in capsaicin-induced mechanical secondary hyperalgesia in mice. Pain 138: 514-524, 2008.
21. Kroth A, Santos MDCQ, Borella da Silva TC, Santos Silveira EM and Partata WA: Aqueous leaf extract from Luehea divaricata Mart. Modulates oxidative stress markers in the spinal cord of rats with neuropathic pain. J Ethnopharmacol 268: 113674, 2021.
22. Long H, Zheng H, Ai L, Osman K and Liu Z: Down-Regulation of NOX4 expression in dorsal horn of spinal cord could alleviate cancer-induced bone pain in rats by reducing oxidative stress response. Cancer Manag Res 12: 10929-10938, 2020.
23. Hussain T, Tan B, Yin Y, Blachier F, Tossou MC and Rahu N: Oxidative stress and inflammation:What polyphenols can do for us? Oxid Med Cell Longev 2016: 7432797, 2016.
24. Duarte A, Silveira GG, Soave DF, Costa JPO and Silva AR: The Role of the LY294002-A non-selective inhibitor of phosphatidylinositol 3-Kinase (PI3K) pathway- in cell survival and proliferation in cell line SCC-25. Asian Pac J Cancer Prev 20: 3377-3383, 2019.
25. Liu Y, Qin X, Lu X and Jiang J: Effects of inhibiting the PI3K/Akt/mTOR signaling pathway on the pain of sciatic endometriosis in a rat model. Can J Physiol Pharmacol 97: 963-970, 2019.

26. Liu W, Lv Y and Ren F: PI3K/Akt pathway is required for spinal central sensitization in neuropathic pain. Cell Mol Neurobiol 38: 747-755, 2018.
27. Jiang B, Zhong X, Fang J, Zhang A, WangD W, Liang Y, Fang J, Chen F and Du J: Electroacupuncture attenuates morphine tolerance in rats with bone cancer pain by inhibiting PI3K/Akt/JNK1/2 signaling pathway in the spinal dorsal horn. Integr Cancer Ther 20: 1534735421995237, 2021.
28. Mao Y, Wang C, Tian X, Huang Y, Zhang Y, Wu H, Yang S, Xu K, Liu Y, Zhang W, *et al*: Endoplasmic reticulum stress contributes to nociception via neuroinflammation in a murine bone cancer pain model. Anesthesiology 132: 357-372, 2020.
29. Liao C, Xu D, Liu X, Fang Y, Yi J, Li X and Guo B: Iridium (III) complex-loaded liposomes as a drug delivery system for lung cancer through mitochondrial dysfunction. Int J Nanomedicine 13: 4417-4431, 2018.
30. Donnelly CR, Andriessen AS, Chen G, Wang K, Jiang C and Maixner W: Central nervous system targets: Glial cell mechanisms in chronic pain. Neurotherapeutics 17: 846-860, 2020.
31. Chatterjee P, Pedrini S, Stoops E, Goozee K, Villemagne VL, Asih PR, Verberk IMW, Dave P, Taddei K, Sohrabi HR, *et al*: Plasma glial fibrillary acidic protein is elevated in cognitively normal older adults at risk of Alzheimer's disease. Transl Psychiatry 11: 27, 2021.
32. Tsuruta F, Masuyama N and Gotoh Y: The phosphatidylinositol 3-kinase (PI3K)-Akt pathway suppresses Bax translocation to mitochondria. J Biol Chem 277: 14040-14047, 2002.
33. Sindhi V and Erdek M: Interventional treatments for metastatic bone cancer pain. Pain Manag 9: 307-315, 2019.
34. Lawton AJ, Lee KA, Cheville AL, Ferrone ML, Rades D, Balboni TA and Abrahm JL: Assessment and management of patients with metastatic spinal cord compression: A multidisciplinary review. J Clin Oncol 37: 61-71, 2019.
35. Laakso H, Lehto LJ, Paasonen J, Salo R, Canna A, Lavrov I, Michaeli S, Gröhn O and Mangia S: Spinal cord fMRI with MB-SWIFT for assessing epidural spinal cord stimulation in rats. Magn Reson Med 86: 2137-2145, 2021.
36. Paolini F, Ferini G, Bonosi L, Costanzo R, Brunasso L, Benigno UE, Porzio M, Gerardi RM, Giammalva GR, Umana GE, *et al*: Spinal cord stimulationto treat unresponsive cancer pain: A possible solution in palliative oncological therapy. Life (Basel) 12: 554, 2022.
37. Bosma RL, Mojarad EA, Leung L, Pukall C, Staud R and Stroman PW: FMRI of spinal and supra-spinal correlates of temporal pain summation in fibromyalgia patients. Hum Brain Mapp 37: 1349-1360, 2016.
38. Zhang R, Lao L, Ren K and Berman BM: Mechanisms of acupuncture-electro acupuncture on persistent pain. Anesthesiology 120: 482-503, 2014.
39. Ji RR, Donnelly CR and Nedergaard M: Astrocytes in chronic pain and itch. Nat Rev Neurosci 20: 667-685, 2019.
40. Wang Y, Kuramitsu Y, Baron B, Kitagawa T, Tokuda K, Akada J, Maehara SI, Maehara Y and Nakamura K: PI3K inhibitor LY294002, as opposed to wortmannin, enhances AKT phosphorylation in gemcitabine-resistant pancreatic cancer cells. Int J Oncol 50: 606-612, 2017.
41. Jo H, Lo PK, Li Y, Loison F, Green S, Wang J, Silberstein LE, Ye K, Chen H and Luo HR: Deactivationof Akt by a small molecule inhibitor targeting pleckstrin homology domain and facilitating Akt ubiquitination. Proc Natl Acad Sci USA 108: 6486-6491, 2011.
42. Yu W, Sun H, Zha W, Cui W, Xu L, Min Q and Wu J: Apigenin attenuates adriamycin-induced cardiomyocyte apoptosis via the PI3K/AKT/mTOR pathway. Evid Based Complement Alternat Med 2017: 2590676, 2017.
43. Sala V, Della Sala A, Ghigo A and Hirsch E: Roles of phosphatidyl inositol 3 kinase gamma (PI3Kγ) in respiratory diseases. Cell Stress 5: 40-51, 2021.
44. Dagia NM, Agarwal G, Kamath DV, Chetrapal-Kunwar A, Gupte RD, Jadhav MG, Dadarkar SS, Trivedi J, Kulkarni-Almeida AA, Kharas F, *et al*: A preferential p110alpha/gamma PI3K inhibitor attenuates experimental inflammation by suppressing the production of proinflammatory mediators in a NF-kappaB-dependent manner. Am J Physiol Cell Physiol 298: C929-C941, 2010.
45. Hellenbrand DJ, Quinn CM, Piper ZJ, Morehouse CN, Fixel JA and Hanna AS: Inflammation after spinal cord injury: A review of the critical timeline of signaling cues and cellular infiltration. J Neuroinflammation 18: 284, 2021.
46. Wojdasiewicz P, Poniatowski ŁA and Szukiewicz D: The role of inflammatory and anti-inflammatory cytokines in the pathogenesis of osteoarthritis. Mediators Inflamm 2014: 561459, 2014.
47. Khutornenko AA, Dalina AA, Chernyak BV, Chumakov PM and Evstafieva AG: The role of dihydroorotate dehydrogenase in apoptosis induction in response to inhibition of the mitochondrial respiratory chain complex III. Acta Naturae 6: 69-75, 2014.
48. Boukalova S, Hubackova S, Milosevic M, Ezrova Z, Neuzil J and Rohlena J: Dihydroorotate dehydrogenase in oxidative phosphorylation and cancer. Biochim Biophys Acta Mol Basis Dis 1866: 165759, 2020.
49. Torraco A, Bianchi M, Verrigni D, Gelmetti V, Riley L, Niceta M, Martinelli D, Montanari A, Guo Y, Rizza T, *et al*: A novel mutation in NDUFB11 unveils a new clinical phenotype associated with lactic acidosis and sideroblastic anemia. Clin Genet 91: 441-447, 2017.
50. Qian Y, Liang X, Kong P, Cheng Y, Cui H, Yan T, Wang J, Zhang L, Liu Y, Guo S, *et al*: Elevated DHODH expression promotes cell proliferation via stabilizing β-catenin in esophageal squamous cell carcinoma. Cell Death Dis 11: 862, 2020.
51. Hatinguais R, Pradhan A, Brown GD, Brown AJP, Warris A and Shekhova E: Mitochondrial reactive oxygen species regulate immune responses of macrophages to aspergillus fumigatus. Front Immunol 12: 641495, 2021.
52. Kirkland RA and Franklin JL: Bax, reactive oxygen, and cytochrome c release in neuronal apoptosis. Antioxid Redox Signal 5: 589-596, 2003.
53. Rabchevsky AG, Michael FM and Patel SP: Mitochondria Focused neurotherapeutics for spinal cord injury. Exp Neurol 330: 113332, 2020.
54. Zhong Z, Umemura A, Sanchez-Lopez E, Liang S, Shalapour S, Wong J, He F, Boassa D, Perkins G, Ali SR, *et al*: NF-κB restricts inflammasome activation via elimination of damaged mitochondria. Cell 164: 896-910, 2016.
55. Cogliati S, Frezza C, Soriano ME, Varanita T, Quintana-Cabrera R, Corrado M, Cipolat S, Costa V, Casarin A, Gomes LC, *et al*: Mitochondrial cristae shape determines respiratory chain supercomplexes assembly and respiratory efficiency. Cell 155: 160-171, 2013.
56. Tian H, Li S and Yu K: DJ-1 alleviates high glucose-induced endothelial cells injury via PI3K/Akt-eNOS signaling pathway. Mol Med Rep 17: 1205-1211, 2018.
57. Liu L, Dong Z, Lei Q, Yang J, Hu H, Li Q, Ji Y, Guo L, Zhang Y, Liu Y and Cui H: Inactivation/deficiency of DHODH induces cell cycle arrest and programed cell death in melanoma. Oncotarget 8: 112354-112370, 2017.